Desalination and Water Treatment
www.deswater.com

doi: 10.5004/dwt.2022.28840

274 (2022) 194–205
October

Comparative biosorption of anions (NO_3^{-1}, SO_4^{-2}, PO_4^{-3}) from aqueous solution in batch system

Candelaria Tejada-Tovar[a,*], Angel Villabona-Ortíz[a], Ángel Darío González-Delgado[b]

[a]*Faculty of Engineering, Process Design and Biomass Utilization Research Group (IDAB), Universidad de Cartagena, Cartagena, Colombia, emails: ctejadat@unicartagena.edu.co (C. Tejada-Tovar), avillabonao@unicartagena.edu.co (A. Villabona-Ortíz)*
[b]*Chemical Engineering Department, Nanomaterials and Computer Aided Process Engineering Research Group (NIPAC), Universidad de Cartagena Avenida del Consulado St. 30, Cartagena de Indias, Colombia, 130015, email: agonzalezd1@unicartagena.edu.co*

Received 11 April 2022; Accepted 10 August 2022

ABSTRACT

The aim of this research is the removal of nitrate, sulfate, and phosphate from aqueous solution using cellulose extracted from *Zea mays* modified with cetyltrimethylammonium chloride evaluating the effect of temperature on the process in batch system. The synthesized cellulose was characterized by thermogravimetric analysis and derivative thermogravimetry, its morphology before and after the modification was performed by scanning electron microscopy-energy-dispersive X-ray spectroscopy. It was evaluated the effect of temperature, finding that at 298 K, it was obtained an adsorption capacity of 19.25, 11.86, and 7.32 mg/g for phosphate, nitrate, and sulfate, respectively. The mechanism of anion adsorption was investigated by fitting the kinetics data to the pseudo-first-order, pseudo-second-order, and Elovich models. The adsorption kinetics was studied and the pseudo-second-order model fitted the data for nitrate and sulfate, while the pseudo-first-order model described the behavior for phosphate. Adsorption equilibrium determined that Freundlich's model adjusted the nitrate and phosphate removal data, and the sulfate data adjusted to Dubinin–Radushkevich's model. The calculated thermodynamic parameters indicate that the adsorption process is spontaneous and exothermic. The multicomponent study evidences the preference of the biomaterial towards phosphate, with competition for the active centers between nitrate and sulfate.

Keywords: Anion adsorption; Cetyltrimethylammonium chloride (CTAC); *Zea mays*

1. Introduction

Sulfur, nitrogen, and phosphorus are essential nutrients required for plant growth. This is because enzymatic reactions and some proteins and amino acids contain these elements [1,2]. Nitrate comes mainly from industrial processes, agricultural runoff, animal waste, and septic systems [3]. The presence of phosphorus in the form of phosphate and its accumulation in water bodies is attributed to several sources, predominantly anthropogenic interventions: domestic and industrial wastewater, detergents, animal excrements, and fertilizers [4]. Meanwhile, sulfur in the form of sulfate enters water bodies artificially thanks to the discharge of wastewater from industrial processes of food production, tanneries, photography, paper, fertilizers [5].

It has been established that the minimum concentration of phosphate, nitrate, and sulfate capable of inducing

* Corresponding author.

eutrophication is 0.02 mg/L [6]. Eutrophication could facilitate the rapid growth of blue and green algae that leads to serious environmental and esthetic problems, destroying the equilibrium of the water and decreasing its quality [7]. In addition, human consumption of these nutrients can cause health effects such as diarrhea, respiratory tract infections, vomiting, hypertension, miscarriage, and methemoglobinemia. Therefore, the US-EPA and the World Health Organization (WHO) establish concentrations of 50 mg/L of nitrate in drinking water [8], 10 μg/L of phosphate [9], and 25 mg/L of sulfate [10]. For this reason, it is necessary to control the concentrations of nitrate, sulfate, and phosphate in wastewater before it is discharged into aquatic environments.

Several technologies have been used to remove sulfates, nitrates, and phosphates from wastewater, such as adsorption [11], chemical reduction, microbial remediation, and membrane techniques (nanofiltration, reverse osmosis, and ultrafiltration) [10]. Among them, adsorption techniques are considered the most preferable methods because of their high efficiency, low cost, simple operating conditions, highly available, and easily regenerated adsorbents [12]. Because of their low cost and easy acquisition, agricultural/plant by-products have begun to be studied as bioadsorbents; among these are sugarcane bagasse [13], the rice husk [14], coconut fiber [15], tea residues [7], peanut shells [16], orange and banana peel [11], sawdust from various trees [17,18], corn waste [19].

Research indicated that plant/agricultural wastes containing high levels of polysaccharides are promising biomaterials for preparing some innovative biosorbents. However, when using traditional adsorbents and agricultural by-products to remove nitrates, sulfates, and phosphates they have low adsorption capacity, due to the anionic nature of the surface of agricultural and agro-industrial wastes, making it necessary to modify the material, to change the characteristics of the biomaterial and may attract anions in solution [7]. Previous studies have shown that chemical or physical modification of adsorbents can improve their removal capacity [19,20]. Protonation [27], the impregnation of metals [6], and the cross-linking of amines [21], have been used to improve the adsorption capacity of nitrates, sulfates, and phosphates from adsorbents. Likewise, there were modified husks of yucca and coconut with epichlorohydrin, N,N-dimethylformamide, pyridine, and diethylamine, to remove nitrate and phosphate present in the solution; finding that quaternized biomaterials are good adsorbents of anions present in aqueous solution. The merits of these biomaterials were based on their low cost, abundant availability, and renewability [19].

In this research, cellulose extracted from *Zea mays* stems was modified with cetyltrimethylammonium chloride and its performance was evaluated for the adsorption of nitrate, sulfate, and phosphate in aqueous solution, taking into account the effect of temperature on the process and determining thermodynamic parameters. It is noteworthy that no studies on the use of this biomass modified with cetyltrimethylammonium chloride (CTAC) for anions removal are reported in the literature, therefore the present study's contributions are considered essential for fulfilling this gap.

2. Materials and methods

2.1. Materials

Merck Millipore analytical grade chemicals were used; the mono-potassium phosphate (KH_2PO_4), sodium nitrate ($NaNO_3$), and potassium sulfate (K_2SO_4) were used to prepare the solutions, the pH of these was adjusted with sodium hydroxide (NaOH) and hydrochloric acid (HCl), 1 M. Cetyltrimethylammonium chloride ($(C_{16}H_{33})N(CH_3)_3Cl$) at 25% was used for the chemical modification of the biomass.

2.2. Preparation and characterization of the bioadsorbent

Zea mays stems were collected as agricultural waste from a local farm. They were washed with deionized water, dried at 60°C for 12 h, reduced in size in an electric mill, and the sizes below 0.14 mm were selected. The cellulose was extracted by placing 20 g of pretreated *Zea mays* stems, in contact with distilled water at a 2% w/v rate and mechanically shaken for 10 min; the mixture was then filtered, the supernatant was discarded, and 500 mL of a 4% w sodium hydroxide solution was added and shaken at 200 rpm at 80°C for 2 h. The sample was then washed with distilled water, the sodium hydroxide treatment was repeated and the sample was washed again until the wash water was clear. The cellulose obtained was dried at room temperature for 8 h. Lignin, polyphenols, and proteins were removed by adding to the sample obtained a solution with 50 g of $NaClO_2$, 500 mL of distilled water, and 50 mL of glacial acetic acid. The mixture was stirred for 24 h at 30°C. A total of 6.2 g of cellulose was obtained, which was dried for 3 h at 60°C [22]. The modification of the cellulose was made by adding 62.8 mL of CTAC at 100 mmol/L; the mixture was kept in magnetic agitation for 24 h at 250 rpm at 27°C, with this it was possible to change the surface of the cellulose thanks to this ammonium salt that acts as an etherifying agent and therefore to reach a positive charge on the surface of the adsorbent [23]. The synthesized cellulose was characterized by thermogravimetric analysis (TGA) and derivative thermogravimetry (DTG) in an SDT Q600 TA Instrument using an inert atmosphere with a nitrogen flow of 4 cm^3/min, in a temperature range of 30°C–600°C at a heating rate with ramp function of 10°C/min. The morphology of the cellulose before and after the modification by using a cationic surfactant, CTAC, was performed by scanning electron microscopy (SEM-EDS). The distribution of loads on the surface and later evaluation of its capacity to remove anionic contaminants was carried out by determining the zero loading point pH (pH_{pzc}) [24].

2.3. Batch adsorption experiments

It was defined an experimental design with temperature as an independent variable with five levels of variation: 298, 303, 308, 313, and 318 K. The adsorption capacity (mg/g) of nitrate, sulfate, and phosphate ions was considered as the dependent variable, and the pH, stirring rate (rpm), initial concentration of the contaminant (mg/L) and the adsorbent dose (g) were considered as intervening variables.

Solutions at 100 mg/L were prepared for the adsorption tests. The phosphate solution was prepared by adding 439 mg of dehydrated KH_2PO_4 in one liter of distilled water [25]. For the sulfate one, 0.1479 g of dehydrated Na_2SO_4 was dissolved in one liter of distilled water [26]. To prepare the nitrate solution was dried in an oven at 103°C–105°C for 24 h; 0.7218 g was dissolved in 1 L of deionized water; the solution was preserved by adding 2 mL of chloroform [27]. The experiments were performed by placing 5 mL of contaminated solution with 0.01 g of adsorbent, at 200 rpm in an orbital shaker at different temperature conditions.

The multi-component adsorption experiments were performed by placing 3 g of adsorbent in 150 mL of equimolar contaminant solution in contact for 24 h; for this, 50 mL of each solution (nitrate, sulfate, and phosphate) was mixed at 100 mg/L. Microfilters of 0.45 nm were used to separate the solution from the adsorbent. The sample for the determination of nitrate and sulfate was stored in plastic vials, while the sample for phosphate was stored in amber glass vials and then refrigerated until analysis.

The detection of the contaminants was made by means of UV-Vis spectrophotometry, Biobase Model BK-UV1900. The detection of phosphate was made at 880 nm determining the blue compound formed by the reaction of ammonium molybdate and antimony and potassium tartrate with orthophosphates in an acid medium to form phosphomolybdic acid. [25]. The sulfate anion was determined at 420 nm, by ion precipitation in the presence of acetic acid and barium chloride [26]. Nitrates were determined at 543 nm by the azo color formed by sulfanilamide and N-(1-Naphthyl)ethylenediamine dichloride [27]. For all the nitrate samples, the correction was made to determine the possible presence of nitrites. The removal efficiency (RE) and the adsorption capacity (q_e), were determined according to Eqs. (1) and (2):

$$\mathrm{RE}(\%) = \frac{C_0 - C_{\mathrm{eq}}}{C_0} \times 100 \tag{1}$$

$$q_e(\mathrm{mg/g}) = \frac{(C_0 - C_{\mathrm{eq}}) \times V}{m} \tag{2}$$

where C_0 and C_{eq} represent the initial concentration of anions in the solutions and the concentration in equilibrium after the adsorption process, both expressed in mg/L. V is the volume of the solution in L and m the amount of adsorbent in g.

2.4. Kinetics and isotherms of adsorption

The kinetic study was conducted to determine the service time of the adsorbent and the mechanisms that control the adsorption process [5]. Kinetic experiments were carried out at best temperature conditions, at 100 mg/L using 0.2 g in 100 mL solution, 200 rpm sampling at 5, 10, 20, 30, 60, 180, 300, 420, and 1,440 min for each assay. The pseudo-first-order, pseudo-second-order, Elovich and intraparticle diffusion, models were adjusted to analyze the experimental kinetic data; their equations and parameters are summarized in Table 1.

Adsorption isotherm describes the phenomena responsible for the process and represents the amount of solute adsorbed per unit mass in the equilibrium [28]. The

Table 1
Kinetic adsorption models [2]

Model	Equation	Parameters
Pseudo-first-order	$q_t = q_e\left(1 - e^{-k_1 t}\right)$	k_1 ($\mathrm{min^{-1}}$): Lagergren's constant q_e (mg/g): the amount of pollutant adsorbed per unit of mass in the equilibrium q_t (mg/g): the amount of pollutant adsorbed per unit of mass at any time t t (min): time
Pseudo-second-order	$q_t = \dfrac{t}{\dfrac{1}{k_2 \times q_e^2} + \dfrac{t}{q_e}}$	k_2 (g/mmol·min): second-order reaction rate coefficient q_e (mg/g): the amount of pollutant adsorbed per unit of mass in the equilibrium q_t (mg/g): the amount of pollutant adsorbed per unit of mass at any time t t (min): time
Elovich	$q_t = \dfrac{1}{\beta} \times \ln(\alpha\beta) + \dfrac{1}{\beta} \times \ln(t)$	α (mg/g·min): initial rate of adsorption β (g/mg): desorption constant related to the surface extent and activation energy for chemisorption q_t (mg/g) which represents the amount of chemisorbed gas in a time t t (min): time
Intraparticle diffusion	$q_t = k_3 t^{0.5} + C$	q_t (mg/g): amount of contaminant adsorbed per mass unit of adsorbent in a time, t t (min): time k_3 ($\mathrm{mg/g \cdot min^{1/2}}$): constant intraparticle diffusion C: boundary layer thickness

experiments were carried out by placing 0.02 g of adsorbent in contact with 100 mL of the solution of the anions for 24 h at different concentrations: 20, 40, 60, 80, and 100 mg/L. Langmuir, Freundlich, and Dubinin–Radushkevich models were used to adjust to the experimental data obtained at equilibrium time. The equations and parameters are summarized in Table 2.

2.5. Thermodynamic parameters

It was determined the change in standard enthalpy ($\Delta H°$), standard entropy ($\Delta S°$), and Gibbs free energy ($\Delta G°$), in order to establish the nature of the process and its behavior with respect to temperature. For this, the Van't Hoff graphical method was implemented, which is summarized in Eqs. (3) and (4):

$$\Delta G° = -RT\mathrm{Ln}\left(K_c\right) \tag{3}$$

$$\mathrm{Ln}\ K_C = \frac{-\Delta H°}{RT} + \frac{\Delta S°}{R} \tag{4}$$

where R is the ideal gas constant and has a value of 8.314 J/mol·K, T is the temperature expressed in Kelvin and K_C is the adsorption equilibrium constant.

3. Results and discussion

3.1. Cellulose characterization

Fig. 1 shows the TGA analysis of the cellulose extracted from the *Zea mays* stems. This analysis provides information about the composition of a sample by monitoring its behavior in relation to temperature in a specific atmosphere, that is, the loss of weight of the sample when exposed to a combination of temperature, heating rate, and reaction atmosphere is recorded [30]. The maximum decomposition temperature was determined from the point where the slope of the thermogravimetric curve begins to change dramatically. The analysis curve shown can be divided into three stages: the first one goes from 30°C to 225°C, where there is a decrease of approximately 10% of mass loss thanks to the evaporation of water molecules. The second stage can be seen from 250°C to 400°C, here the most significant loss of mass is about 70%, and corresponds to the loss of hemicellulose and lignin [31]. Finally, from 400°C to 600°C there is still a decrease in the mass of the sample, approximately 21% and it corresponds to the degradation of non-cellulosic substances [31]. From the results, it is evident that the sample is constituted in greater proportion by cellulose, considering that up to 200°C humidity evaporates, mass losses between 200°C and 400°C are due to the decomposition of cellulose and hemicellulose, and at temperatures above 580°C losses are due to the decomposition of lignin and the possible presence of stable oxides at high temperatures [32]. It has been reported that lignin is the most difficult component to decompose with temperature; its decomposition generally extends over the entire temperature range from approximately 200°C to 500°C [33].

The curve of the cellulose DTG analysis shown in Fig. 2, shows exothermic pyrolysis of almost all the material, except for a large and evident endothermic peak that occurs around 360°C, which may be due to the degradation of cellulose molecules. This result is congruent with the characterization of lignocellulosic materials performed by Díez et al. [31], where commercial cellulose presents a similar behavior. Lignin decomposes between 200°C and 500°C, however, it did not form a peak because the various functional oxygen groups generated during lignin decomposition had different thermal stabilities. The non-appearance of a peak between 222°C–228°C indicates

Table 2
Isothermal models [29]

Model	Equation	Parameters
Langmuir	$q_e = \frac{q_{\max} K_L C_e}{1 + K_L C_e}$	C_e (mg/L): concentration of the adsorbate in the equilibrium q_e (mg/g) amount of adsorbate adsorbed per gram of adsorbent at equilibrium $q_{\max}$ (mg/g): coverage capacity in the monolayer K_L: Langmuir isothermal constant
Freundlich	$q_e = K_F C_e^{1/2}$	q_e (mg/g): the amount of adsorbate adsorbed per gram of adsorbent in the equilibrium K_F (L/g): Freundlich's isothermal constant C_e (mg/L): concentration of adsorbate in the equilibrium
Dubinin–Radushkevich	$q_e = q_{\mathrm{DR}} \times e^{-K_{\mathrm{DR}}\varepsilon^2}$ $E = \frac{1}{\sqrt{2K_{DR}}}$ $\varepsilon = RT \times \ln\left(1 + \frac{1}{C_e}\right)$	ε^2: Polanyi's potential which is based on the temperature K_{DR} (mol²/kJ²): Dubinin–Radushkevich's constant related to adsorption energy E (kJ/mol): is the average adsorption energy per molecule of adsorbate required to transfer one mole of the ion from the solution to the surface of the adsorbent

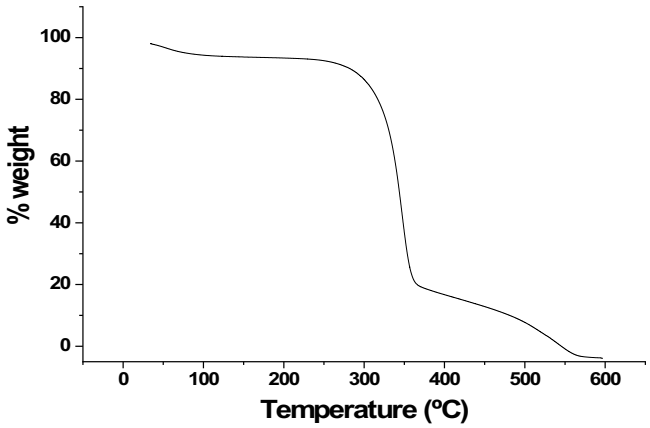

Fig. 1. TGA analysis of *Zea mays* stem cellulose.

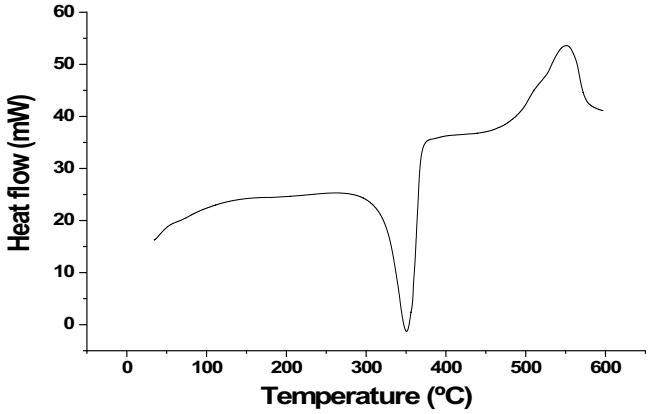

Fig. 2. Calorimetric analysis.

that the hemicellulose was removed during the process of extracting the cellulose from the *Zea mays* stems [31].

The morphology of the cellulose extracted from the stems of *Zea mays* before and after the modification by the use of cationic surfactant, CTAC, was observed by SEM with ×1,000 magnification; the micrographs are shown in Fig. 3. It is observed that the surface structures and porosity can be seen, due to the delignification of the corn stems [33]. The morphology of the unmodified cellulose surface was slightly different after the modification; no significant increase is observed in the porosity and therefore, the physicochemical properties of the biomaterial [34]. The EDS spectrum of the cellulose showed the peaks of carbon (53.29 wt.%) and oxygen (46.71 wt.%), corresponding to its bond energies, without the presence of impurities which confirms the quality of the synthesized cellulose that was evident in the TGA of Fig. 1 [7]. However, there is a change in the exposed surface of the material after the modification, increasing the roughness of the material, and the softening of the surface due to the dissolution of impurities [35], EDS does not evidence that this has been carried out satisfactorily; there was a decrease in the presence of carbon (52.17% w) and oxygen (47.69% w) and traces of aluminum (0.14% w) in the peak intensity 1.5 keV. Previously, corn husk and jackfruit peels residues modified with N,N-dimethylformamide, ethylenediamine, and triethylamine, finding that a high percentage of nitrogen was presented in the surface of the modified material, verifying that the group of quaternary ammonia (NR^{4+}) reacted in the exposed surface of the material, giving as result a successful synthesis [19].

The zero pH charge point of CTAC-modified cellulose was determined to establish the ideal pH for anion adsorption. A graph of the initial pH vs. the final pH is shown in Fig. 4. The bioadsorbent acts as a positively charged matrix at pH values below pH_{pzc}; if the pH of the solution is increased and it could bind to nitrate, sulfate, and phosphate ions, it would behave similarly to negative species due to deprotonation of surface functional groups and would reject interaction with the anions under study due to their electrostatic charges [3]. The pH_{pzc} of *Zea mays* stem cellulose modified with CTAC was 6.06, indicating that pH values below this value should have a positively charged surface. Thus, the adsorption essays were carried put at pH 4.

3.2. Thermodynamic study

Fig. 5 shows that the highest adsorption capacity of the three nutrients is obtained at 298 K, which indicates that the process does not need an energy supply to be carried out due to the possible exothermic nature of the reactions. The selectivity of the bioadsorbent under study by the phosphate anion is observed, which could be due to the adsorption of additional H^+ from the solution on the surface of the modified cellulose, thus its net charge becomes positive and causes a high adsorption capacity of the anions [36].

Table 3 summarizes the thermodynamic parameters of nitrate, sulfate, and phosphate adsorption. The positive values of $\Delta G°$ indicate that the system is not spontaneous for the removal of anions using the synthesized biochar, furthermore the fact that the $\Delta G°$ increases as the temperature of the system increases the process energetically becomes more favorable [36]. It is established that the removal of nitrate and sulfate is exothermic due to the negative sign of $\Delta H°$, therefore it is not necessary to provide energy to the system during the process [37]. The negative value of $\Delta S°$ indicates the irreversibility of the removal of nitrate and sulfate, and a low probability of structural changes due to the formation of the bonds between the active centers of the bioadsorbent and the contaminants [38].

3.3. Adsorption kinetics

Adsorption kinetics was studied to determine the effect of contact time on the process and the possible mechanisms involved during removal [12]. The fitting of the experimental data to the Elovich, pseudo-first-order, pseudo-second-order and intraparticle diffusion models is shown in Fig. 6.

The adsorption of the three anions in the bioadsorbent occurs rapidly in the initial stages of the process and then gradually decreases. This is due to the availability of active sites for adsorption that decreases as they become saturated; and accordingly with Balarak et al. [36], the high concentration of the dye at the onset of adsorption helps in creating a better mass transfer driving force, overcoming the resistance to external diffusion; hence, the accelerated

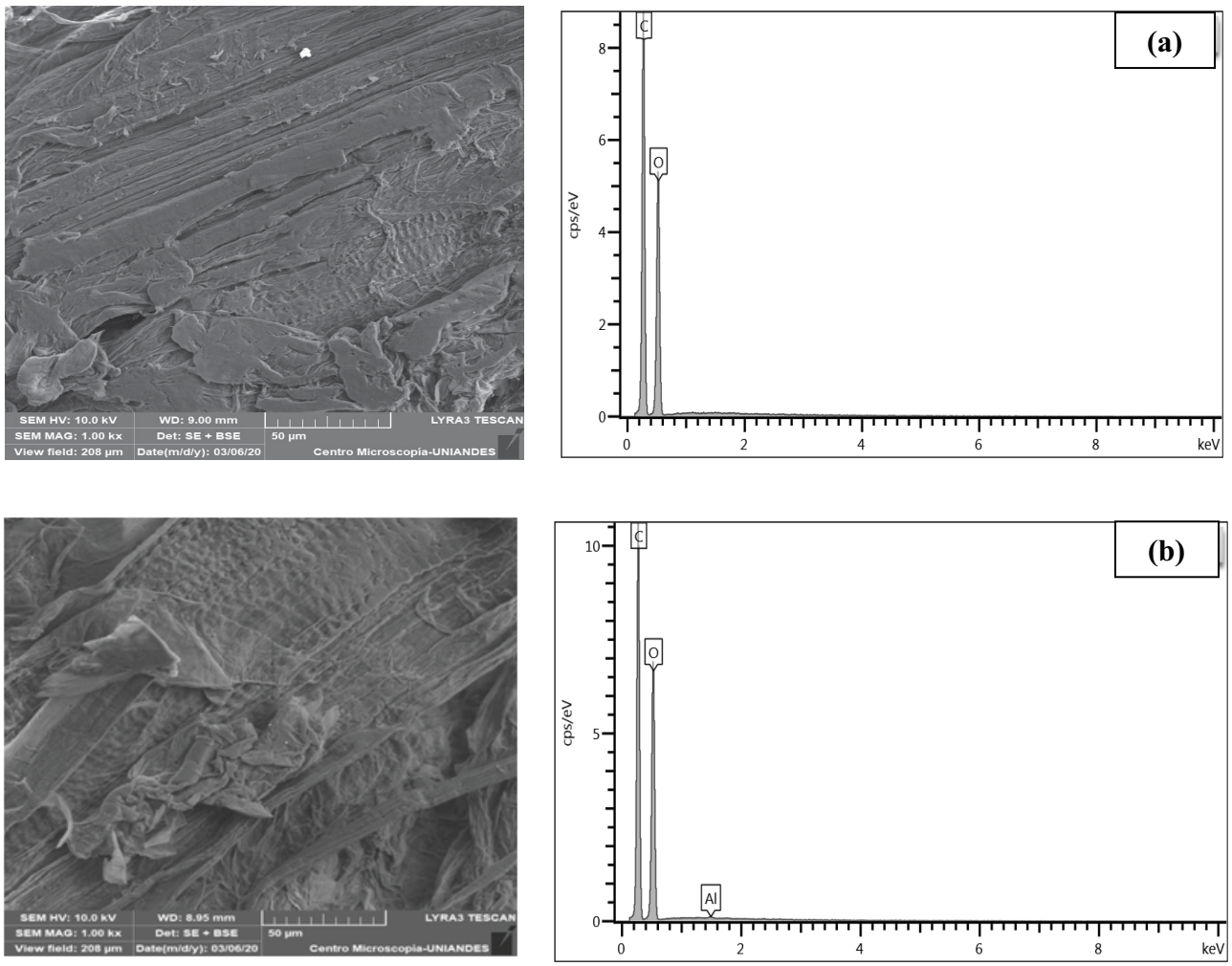

Fig. 3. SEM-EDS spectrum of cellulose (a) unmodified and (b) modified with CTAC.

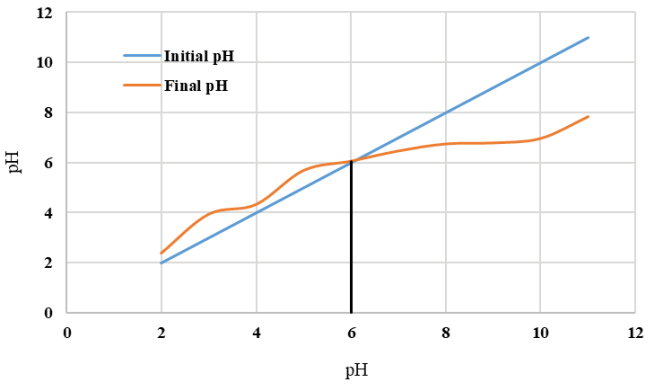

Fig. 4. pH_{pzc} of CTAC-modified cellulose.

adsorption rate. It is observed that equilibrium is reached at about 420 min for the three anions, confirming the preference of the adsorbent for phosphate.

As summarized in Table 4, as well as the adjustment shown in Fig. 6, the pseudo-second-order model best describes the kinetics of nitrate and sulfate removal, suggesting that the mechanism by which adsorption occurs is chemical, in which the rate of adsorption is limited by valence forces given by the exchange of electrons between the adsorbate and the adsorbent. On the other hand, phosphate data was better adjusted by the pseudo-first-order model which indicates that adsorption occurs in one active center at a time [12].

The intraparticle diffusion model was used to study the adsorption mechanism, to define the rate-limiting step of the adsorption process. Considering the plots shown in Fig. 7, it can be said that lines pass through the origin, then intraparticle diffusion was the only rate-limiting step. Nevertheless, this is not the only limiting step, taking into account that kinetics may be controlled by a combination of intra-particle diffusion and film diffusion [37]. The lines for the nitrates, sulfate, and phosphate, show three stages being the first one the fastest; this stage shows increased adsorption due of the diffusion from the bulk of the solution to the boundary of the adsorbent. The second stage shows a diminution in the rate of adsorption. The third stage is considered the slowest; it may be dominated by intraparticle diffusion through

Table 3
Thermodynamic adsorption parameters

Contaminant	Temperature (K)	$\Delta H°$ (kJ/mol·K)	$\Delta S°$ (kJ/mol)	$\Delta G°$ (kJ/mol)
	298			8.9174
	303			9.1689
Phosphate	308	6.0789	0.0503	9.4204
	313			9.6719
	318			9.9234
	298			10.3716
	303			10.9179
Nitrate	308	–22.2025	–0.1093	11.4642
	313			12.0104
	318			12.5567
	298			11.8795
	303			12.5075
Sulfate	308	–25.5705	–0.1256	13.1355
	313			13.7636
	318			14.3916

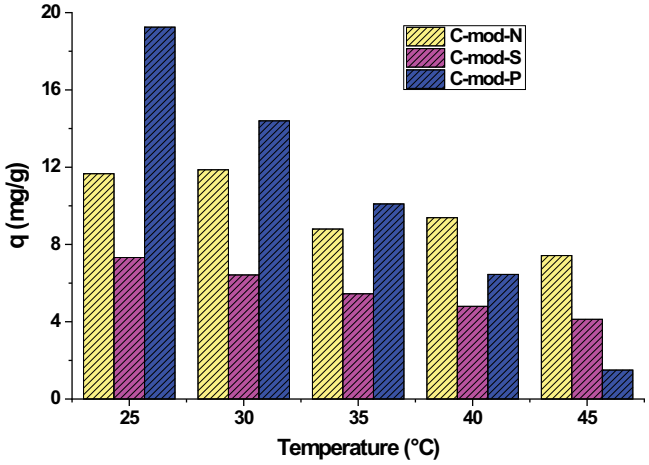

Fig. 5. Effect of temperature on the adsorption capacity of nitrate, sulfate, and phosphate on CTAC-modified cellulose.

adsorbent pores; also, equilibrium was established at this stage [39].

3.4. Adsorption equilibrium

Adsorption equilibrium was performed by studying the isotherms at the best experimental temperature condition (298 K), at initial concentrations of 20, 40, 60, 80, and 100 mg/L. Fig. 8 shows the adjustment to Langmuir, Freundlich, and Dubinin–Radushkevich models, made by nonlinear regression of the nitrate, sulfate, and phosphate adsorption isotherms on the cellulose of *Zea mays* stems modified with CTAC. The parameters are summarized in Table 5. The best-fitting was chosen according to the determined correlation coefficient (R^2) and the sum of errors (SS).

As shown in Table 5, the Freundlich's model is the one that best adjusts the nitrate and phosphate adsorption equilibrium data, with R^2 of 0.95 and 0.98, respectively. The above suggests that the adsorption of the two anions on the cellulose of *Zea mays* stems modified with CTAC gives a multilayer adsorption thanks to the heterogeneous surface [40]. On the other hand, the data of the sulfate isotherm were adjusted to Dubinin–Radushkevich's model; the value registered for E suggests that the process is mostly controlled by the mechanism of ion exchange with strong interactions between the active centers and the anion since they exceed 8 kJ/mol. The adjustment to Dubinin–Radushkevich's model assumes that the bioadsorbent presents a heterogeneous structure [3]. Karthikeyan and Meenakshi [3], found that Freundlich's model described the adsorption of phosphate and nitrate.

Table 6 summarizes the q_{max} values obtained in previous studies and the present research for the adsorption of nitrate (NO_3^-), sulfate (SO_4^{2-}), and phosphate (PO_4^{3-}) onto adsorbents of different nature. It is observed that the results obtained in the present study for the removal of NO_3^- are in the interval reported from 5 mg/g up to 68.96 mg/g, for PO_4^3 they are between 19.24 and 46.67 mg/g, being the lowest reported in the present study; finally, the capacities obtained when removing SO_4^{2-} are in the range of 8.38 and 78.10 mg/g. It is evidenced that the most effective modifications involve the quaternization of bioadsorbents with, epichlorohydrin, pyridine, and quaternary salts as N,N-dimethylformamide, trimethylamine, diethylamine. When comparing the removal of NO_3^- with an activated carbon modified with CTAC at 25%, also used in this study, it is found that the capacity obtained with cellulose from corn stalks is higher [23].

3.5. Multicomponent adsorption tests

The competitive study was conducted by means of a batch system test using an equimolar ternary solution of nitrate, sulfate, and phosphate at 298 K with an adsorbent dose of 0.03 g in 150 mL of solution. Fig. 9 shows

Table 4
Adjustment parameters of kinetic models

Model	Parameter	Nitrate	Sulfate	Phosphate
Pseudo-first-order	k_1 (min^{-1})	0.0147	0.0258	0.0073
	q_e (mg/g)	11.2036	6.8739	19.6829
	R^2	0.9741	0.9730	0.9867
	SS	0.3878	0.1956	0.6884
Pseudo-second-order	k_2 (g/mg·min)	0.0014	0.0045	3.60E-04
	q_e (mg/g)	12.5699	7.4891	22.9392
	R^2	0.9827	0.9975	0.9629
	SS	0.4398	0.0764	1.6274
Elovich	α (mg/g·min)	0.6375	0.7856	0.5361
	β (g/mg)	0.4523	0.9199	0.2392
	R^2	0.9430	0.9455	0.9013
	SS	0.0394	0.0697	0.0261
Intraparticle diffusion	k_3	1.4489	2.1739	3.2540
	C	30.2155	53.1515	72.1516
	R^2	0.8885	0.8721	0.7725
	SS	0.7960	2.6571	15.7333

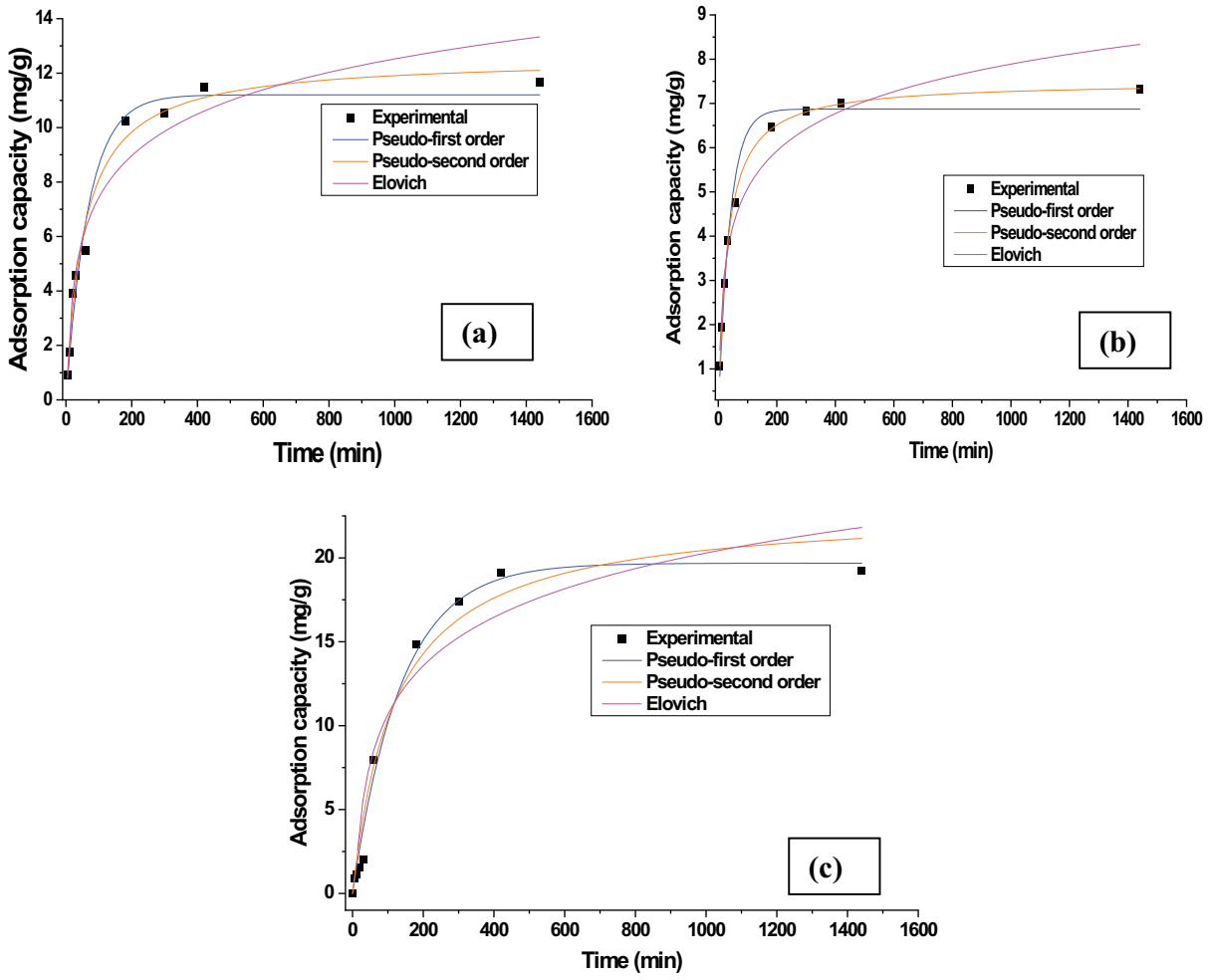

Fig. 6. Kinetics of the adsorption of (a) nitrate, (b) sulfate, and (c) phosphate.

Table 5
Adjustment parameters of isothermal models

Model	Parameter	Nitrate	Sulfate	Phosphate
Langmuir	q_{max} (mg/g)	20,562.6295	1,900	55,695.0645
	K_L (L/mg)	7.32E-06	5.16E-05	5.03E-06
	R^2	0.9196	0.7014	0.8792
	SS	1.232	0.515	8.0491
Freundlich	K_F (mg/g)	0.0526	0.0627	0.0366
	n	0.7957	0.9041	0.6573
	R^2	0.9546	0.7081	0.9832
	SS	0.162	2.4849	0.0838
Dubinin–Radushkevich	q_{DR} (mg/g)	15.7772	10.7359	23.9215
	K_{DR} (mol²/kJ²)	2.3514E-04	2.4493E-04	1.5645E-04
	E (kJ/mol)	46.0864	45.1819	56.5324
	R^2	0.94	0.8465	0.9389
	SS	1.8539	2.1699	3.1143

Table 6
Comparison of q_{max} values

Contaminant	Adsorbent	q_{max} (mg/g)	Reference
NO_3^-	Zn–Al LDHs/activated carbon composite	73.742	[3]
	Amine cross-linked tea waste	136.43	[7]
	Polyurethane/sepiolite cellular nanocomposites	23.30	[40]
	Corn husk quaternized with N,N-dimethylformamide, ethylenediamine, and triethylamine	79.09	[19]
	Jackfruit peel quaternized with N,N-dimethylformamide, ethylenediamine, and triethylamine	62.91	
	Cetylpyridinium bromide modified zeolite	28.06	[12]
SO_4^{2-}	Manure biochar	78.4	[1]
	Manganite	16.4	[5]
NO_3^-	Unmodified activated carbon	3.86	[23]
	25% CTAC-modified activated carbon	7.1	
	Activated carbon modified with CTAC at 50%	10.5	
	100% CTAC-modified activated carbon	14.3	
PO_4^{3-}	Strontium magnetic graphene oxide nanocomposite	238.09	[2]
SO_4^-	Clinoptilolite	74.63	[6]
	Magnetic nanotubes	94	
PO_4^{3-}	Zirconium hydroxide encapsulated in quaternized cellulose	83.6	[21]
NO_3^-	*Zea mays* stem cellulose modified with cetyltrimethylammonium chloride	11.663	Present study
SO_4^{2-}		8.38	
PO_4^{3-}		19.24	

increased selectivity by the modified cellulose towards the phosphate anion, which can be attributed to the trivalent nature of the anion which potentially gives it a higher selectivity. Nitrate was the least removed, which could be due to its monovalent nature, so it would have a higher selectivity for specific active centers of the bioadsorbent, thus decreasing its removal by competing for adsorption sites with phosphate and sulfate [12].

Anions like sulfate, phosphate and nitrate are normally present in drinking water and can compete for the adsorption on the available vacant sites. Typically, to occupy the active adsorption site sulfate ions have a high interest to compete with phosphate and nitrate ions, which will eventually leads to reduce the phosphate and nitrate uptake efficiency [3].

4. Conclusion

This study concluded that: (i) *Zea mays* stem agricultural residue is an abundant agricultural residue and is

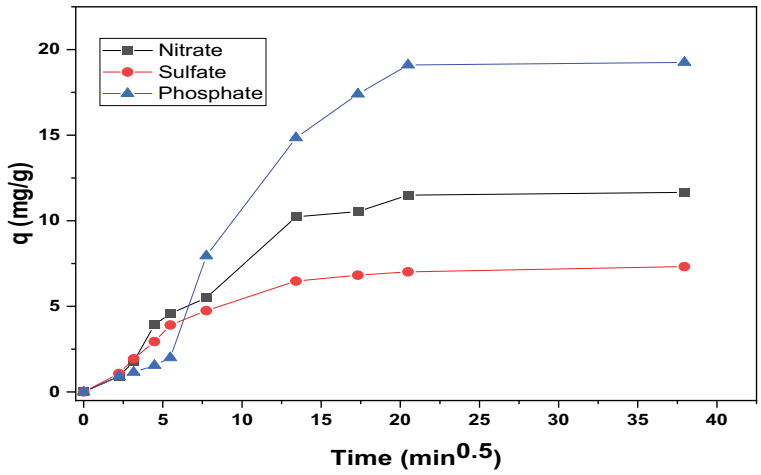

Fig. 7. Intraparticle diffusion kinetic plots for nitrate, sulfate, and phosphate adsorption.

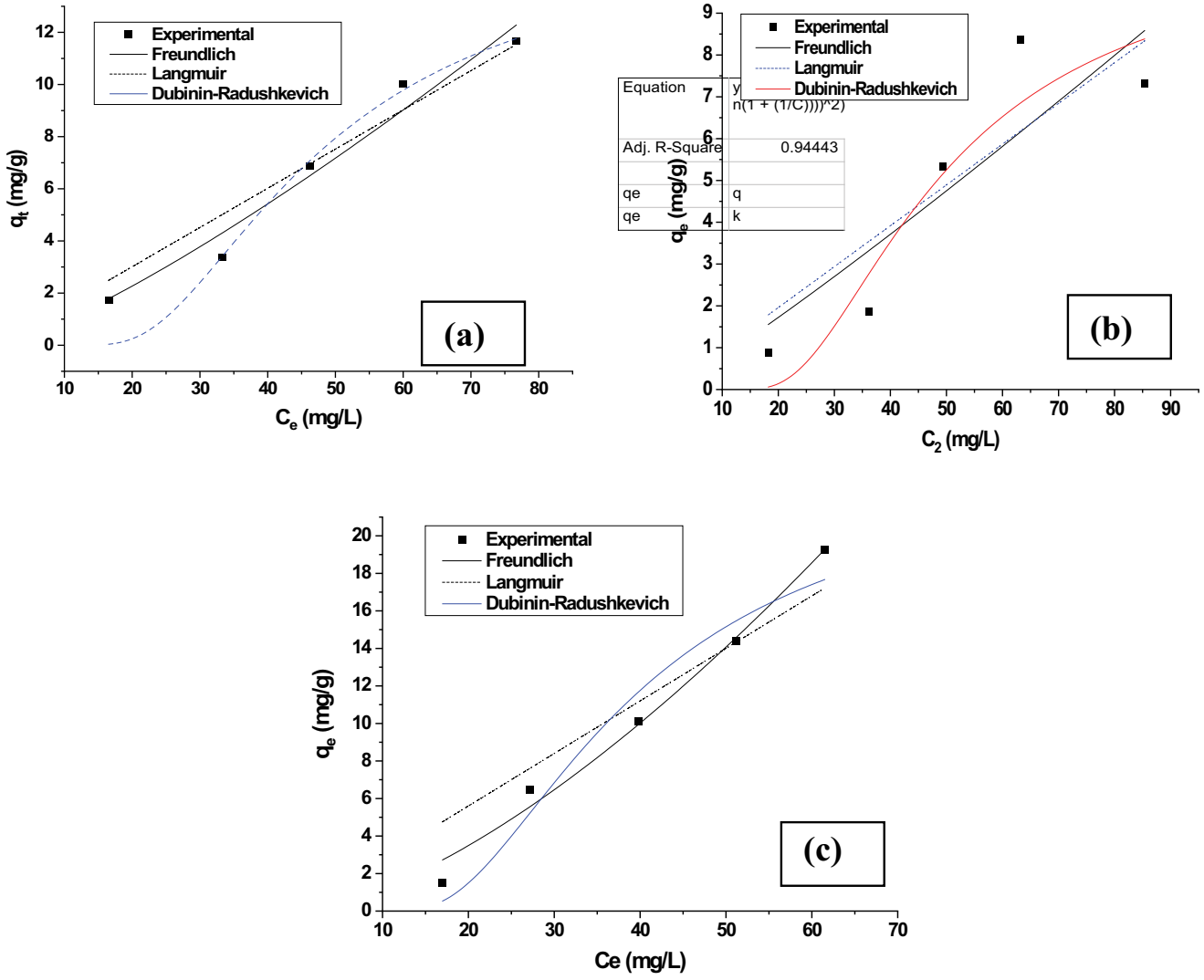

Fig. 8. Fitting to isothermal models of adsorption equilibrium data of (a) nitrate, (b) sulfate, and (c) phosphate.

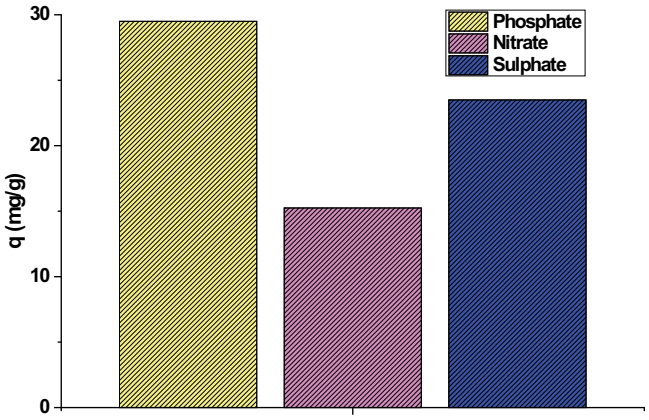

Fig. 9. NO_3^{-1}, SO_4^{-2}, PO_4^{-3} adsorption capacity in multicomponent adsorption.

a good source for the extraction of cellulose as shown by TGA and DTG analyses and that the modification with CTAC performed to protonate the surface of the material was efficient for its use in the removal of the anions under study. (ii) The characterization showed a good quality extracted cellulose, composed mostly of cellulose with traces of lignin and hemicellulose. The analysis (SEM) showed that the surface structures and porosity can be seen, due to the delignification of the corn stems. The EDS spectrum of the cellulose showed the carbon and oxygen peaks corresponding to its binding energies, without the presence of impurities, which confirmed the quality of the synthesized cellulose. After modification by extension with (CTAC), a change in the exposed surface of the material was observed, increasing the roughness of the material and favoring the capture of anions. (iii) The effect of temperature was evaluated and it was found that at 298 K the highest adsorption capacity of 19.25, 11.86, and 7.32 mg/g was obtained for phosphate, nitrate, and sulfate, respectively. (iv) Adsorption kinetics showed that equilibrium was reached at 420 min and that the pseudo-second-order model adjusted the data of nitrate and sulfate, while the pseudo-first-order model described the behavior for phosphate; the adsorption equilibrium determined that the Freundlich model adjusts the nitrate and phosphate removal data, indicating that the process occurs in multi layers; on the other hand, the sulfate data adjusted to Dubinin–Radushkevich's model establishing that the mechanism that controls the process is the ion exchange between the anion and the active centers of the biomaterial. (v) The calculated thermodynamic parameters indicate that the adsorption process is spontaneous and exothermic and that the multi-component study evidences the preference of the biomaterial for phosphate, without indicating competition for the active centers of the material among the anions studied.

Acknowledgments

The authors thank the University of Cartagena for providing financial support to conclude this work.

Symbols

q_e	—	Adsorption capacity at equilibrium, mmol/g
q_t	—	Adsorption capacity at a t time
k_1	—	Constant of the rate of pseudo-first-order reaction, min^{-1}
k_2	—	Constant of the rate of reaction pseudo-second-order, g/min
α	—	Elovich initial adsorption rate, mg/g·min
β	—	Elovich constant, g/mg
q_e	—	Adsorbed metal concentration on the adsorbent, mg/g
C_e	—	Residual metal concentration in solution, mg/L
q_{max}	—	Maximum adsorption which corresponds to saturation sites, mg/g
K_F	—	Freundlich constant, mg/L·g^2
n	—	Adsorption intensity
q_e	—	Amount of adsorbate captured on the adsorbent, mg/g
k_3	—	Intraparticle diffusion constant, mg/g·$min^{1/2}$

References

[1] B. Zhao, H. Xu, F. Ma, T. Zhang, X. Nan, Effects of dairy manure biochar on adsorption of sulfate onto light sierozem and its mechanisms, RSC Adv., 9 (2019) 5218–5223.
[2] H. Sereshti, E. Zamiri Afsharian, M. Esmaeili Bidhendi, H. Rashidi Nodeh, M. Afzal Kamboh, M. Yilmaz, Removal of phosphate and nitrate ions aqueous using strontium magnetic graphene oxide nanocomposite: isotherms, kinetics, and thermodynamics studies, Environ. Prog. Sustainable Energy, 39 (2020) e13332, doi: 10.1002/ep.13332.
[3] P. Karthikeyan, S. Meenakshi, Synthesis and characterization of Zn–Al LDHs/activated carbon composite and its adsorption properties for phosphate and nitrate ions in aqueous medium, J. Mol. Liq., 29 (2019) 111766, doi: 10.1016/j.molliq.2019.111766.
[4] S.P. Boeykens, N. Redondo, R. Alvarado Obeso, N. Caracciolo, C. Vázquez, Chromium and lead adsorption by avocado seed biomass study through the use of total reflection X-ray fluorescence analysis, Appl. Radiat. Isot., 153 (2019) 108809, doi: 10.1016/j.apradiso.2019.108809.
[5] L. Qiu, G.R. Burton, S. Rousseau, J. Qian, Kinetics and thermodynamics of sulfate adsorption on magnetite at elevated temperatures, J. Solution Chem., 48 (2019) 1488–1502.
[6] A.H. Salami, H. Bonakdari, A. Akhbari, A. Shamshiri, S.F. Mousavi, S. Farzin, M.R. Hassanvand, A. Noori, Performance assessment of modified clinoptilolite and magnetic nanotubes on sulfate removal and potential application in natural river samples, J. Inclusion Phenom. Macrocyclic Chem., 97 (2020) 51–63.
[7] H. Qiao, L. Mei, G. Chen, H. Liu, C. Peng, F. Ke, R. Hou, X. Wan, H. Cai, Adsorption of nitrate and phosphate from aqueous solution using amine cross-linked tea wastes, Appl. Surf. Sci., 483 (2019) 114–122.
[8] WHO, Nitrate and Nitrite in Drinking-Water, World Health Organization, 2019.
[9] United States Environmental Protection Agency, US-EPA, 2018 Edition of the Drinking Water Standards and Health Advisories Tables, 2018.
[10] M.K. Sharma, M. Kumar, Sulfate contamination in groundwater and its remediation: an overview, Environ. Monit. Assess., 192 (2020) 74, doi: 10.1007/s10661-019-8051-6.
[11] P. Venkata Naga Sai Kiran, M.N. Ramu, V.S.B. Nagendra, J.S.R. Krishna, Removal of nitrates from water by environmental waste materials, Int. J. Eng. Res. Appl., 12 (2022) 48–52.
[12] O. Alagha, M.S. Manzar, M. Zubair, I. Anil, N.D. Mu'azu, A. Qureshi, Comparative adsorptive removal of phosphate and nitrate from wastewater using biochar-MgAl LDH

nanocomposites: coexisting anions effect and mechanistic studies, Nanomaterials, 10 (2020) 336, doi: 10.3390/nano10020336.
[13] P. Mehrabinia, E. Ghanbari-Adivi, R. Fattahi, H.A. Samimi, J. Kermanezhad, Nitrate removal from agricultural effluent using sugarcane bagasse active nanosorbent, J. Appl. Water Eng. Res., 10 (2022) 238–249.
[14] N. Sooksawat, S. Santibenchakul, M. Kruatrachue, D. Inthorn, Recycling rice husk for removal of phosphate and nitrate from synthetic and swine wastewater: adsorption study and nutrient analysis of modified rice husk, J. Environ. Sci. Health. Part A Toxic/Hazard. Subst. Environ. Eng., 56 (2021) 1080–1092.
[15] P. Chakraborty, S. Show, W. Ur Rahman, G. Halder, Linearity and non-linearity analysis of isotherms and kinetics for ibuprofen remotion using superheated steam and acid modified biochar, Process Saf. Environ. Prot., 126 (2019) 193–204.
[16] F. Tomul, Y. Arslan, B. Kabak, D. Trak, E. Kendüzler, E.C. Lima, H.N. Tran, Peanut shells-derived biochars prepared from different carbonization processes: comparison of characterization and mechanism of naproxen adsorption in water, Sci. Total Environ., 20 (2020) 137828, doi: 10.1016/j.scitotenv.2020.137828.
[17] P. Patel, S. Gupta, P. Mondal, Modeling of continuous adsorption of greywater pollutants onto sawdust activated carbon bed integrated with sand column, J. Environ. Chem. Eng., 10 (2022) 107155, doi: 10.1016/j.jece.2022.107155.
[18] I. Fatima, M. Ahmad, M. Vithanage, S. Iqbal, Abstraction of nitrates and phosphates from water by sawdust- and rice husk-derived biochars: their potential as N- and P-loaded fertilizer for plant productivity in nutrient deficient soil, J. Anal. Appl. Pyrolysis, 155 (2021) 105073, doi: 10.1016/j.jaap.2021.105073.
[19] H.A.T. Banu, P. Karthikeyan, S. Meenakshi, Comparative studies on revival of nitrate and phosphate ions using quaternized corn husk and jackfruit peel, Bioresour. Technol. Rep., 8 (2019) 100331, doi: 10.1016/j.biteb.2019.100331.
[20] Y. Gao, S.-Q. Deng, X. Jin, S.-L. Cai, S.-R. Zheng, W.-G. Zhang, The construction of amorphous metal-organic cage-based solid for rapid dye adsorption and time-dependent dye separation from water, Chem. Eng. J., 357 (2019) 129–139.
[21] S. Dong, Q. Ji, Y. Wang, H. Liu, J. Qu, Enhanced phosphate removal using zirconium hydroxide encapsulated in quaternized cellulose, J. Environ. Sci., 89 (2020) 102–122.
[22] A.Y. Melikoğlu, S.E. Bilek, S. Cesur, Optimum alkaline treatment parameters for the extraction of cellulose and production of cellulose nanocrystals from apple pomace, Carbohydr. Polym., 215 (2019) 330–337.
[23] F. Xia, H. Yang, L. Li, Y. Ren, D. Shi, H. Chai, H. Ai, Q. He, L. Gu, Enhanced nitrate adsorption by using cetyltrimethylammonium chloride pre-loaded activated carbon, Environ. Technol., 41 (2020) 3562–3572.
[24] A. Herrera-Barros, C. Tejada-Tovar, A. Villabona-Ortíz, A.D. Gonzalez-Delgado, J. Benitez-Monroy, Cd(II) and Ni(II) uptake by novel biosorbent prepared from oil palm residual biomass and Al_2O_3 nanoparticles, Sustainable Chem. Pharm., 15 (2020) 100216, doi: 10.1016/j.scp.2020.100216.
[25] ASTM, ASTM D 515-60 Standard Test Method for Phosphate Ion in Water, American Society for Testing and Materials, 2018, pp. 1–4.
[26] ASTM, ASTM D 4130-15 Standard Test Method for Sulfate in Brackish Water, Seawater, and Brines, American Society for Testing and Materials, 2018, pp. 1–5.
[27] ASTM, ASTM D7781-14 Standard Test Method for Nitrite-Nitrate in Water by Nitrate Reductase, American Society for Testing and Materials, 2018, pp. 1–8.
[28] H. Ao, W. Cao, Y. Hong, J. Wu, L. Wei, Adsorption of sulfate ion from water by zirconium oxide-modified biochar derived from pomelo peel, Sci. Total Environ., 708 (2020) 135092, doi: 10.1016/j.scitotenv.2019.135092.
[29] S. Singh, S. Perween, A. Ranjan, Dramatic enhancement in adsorption of congo red dye in polymer-nanoparticle composite of polyaniline-zinc titanate, J. Environ. Chem. Eng., 9 (2021) 105149, doi: 10.1016/j.jece.2021.105149.
[30] H.A.T. Banu, P. Karthikeyan, S. Vigneshwaran, S. Meenakshi, Adsorptive performance of lanthanum encapsulated biopolymer chitosan-kaolin clay hybrid composite for the recovery of nitrate and phosphate from water, Int. J. Biol. Macromol., 154 (2020) 188–197.
[31] D. Díez, A. Urueña, R. Piñero, A. Barrio, T. Tamminen, Determination of hemicellulose, cellulose, and lignin content in different types of biomasses by thermogravimetric analysis and pseudocomponent kinetic model (TGA-PKM method), Processes, 8 (2020) 1048, doi: 10.3390/pr8091048.
[32] W. Wang, S. Yang, A. Zhang, Z. Yang, Preparation and properties of novel corn straw cellulose–based superabsorbent with water-retaining and slow-release functions, J. Appl. Polym. Sci., 137 (2020) 48951, doi: 10.1002/app.48951.
[33] Y. Liu, J. Xie, N. Wu, Y. Ma, C. Menon, J. Tong, Characterization of natural cellulose fiber from corn stalk waste subjected to different surface treatments, Cellulose, 26 (2019) 4707–4719.
[34] D. Ranjbar, M. Raeiszadeh, L. Lewis, M.J. MacLachlan, S.G. Hatzikiriakos, Adsorptive removal of Congo red by surfactant modified cellulose nanocrystals: a kinetic, equilibrium, and mechanistic investigation, Cellulose, 27 (2020) 3211–3232.
[35] H.K. Chen, S.K. Sharma, P.R. Sharma, K. Chi, E. Fung, K. Aubrecht, N. Keroletswe, S. Chigome, B.S. Hsiao, Nitro-oxidized carboxycellulose nanofibers from moringa plant: effective bioadsorbent for mercury removal, Cellulose, 28 (2021) 8611–8628.
[36] D. Balarak, M. Zafariyan, C.A. Igwegbe, K.K. Onyechi, J.O. Ighalo, Adsorption of Acid Blue 92 dye from aqueous solutions by single-walled carbon nanotubes: isothermal, kinetic, and thermodynamic studies, Environ. Process., 8 (2021) 869–888.
[37] T.J. Al-Musawi, N. Mengelizadeh, O. Al Rawi, D. Balarak, Capacity and modeling of Acid Blue 113 dye adsorption onto chitosan magnetized by Fe_2O_3 nanoparticles, J. Polym. Environ., 30 (2022) 344–359.
[38] Q. Yin, M. Liu, H. Ren, Biochar produced from the co-pyrolysis of sewage sludge and walnut shell for ammonium and phosphate adsorption from water, J. Environ. Manage., 249 (2019) 109410, doi: 10.1016/j.jenvman.2019.109410.
[39] M. Yilmaz, T.J. Al-Musawi, M. Khodadadi Saloot, A.D. Khatibi, M. Baniasadi, D. Balarak, Synthesis of activated carbon from *Lemna minor* plant and magnetized with iron(III) oxide magnetic nanoparticles and its application in removal of ciprofloxacin, Biomass Convers. Biorefin., (2022) 1–14, doi: 10.1007/s13399-021-02279-y.
[40] S. Barroso-Solares, B. Merillas, P. Cimavilla-Román, M.A. Rodriguez-Perez, J. Pinto, Enhanced nitrates-polluted water remediation by polyurethane/sepiolite cellular nanocomposites, J. Cleaner Prod., 254 (2020) 120038, doi: 10.1016/j.jclepro.2020.120038.